32nd URSI GASS, Montreal, 19-26 August 2017

Activation Thresholds for Electrostimulation by TMS and DES: Brain Mapping via Multiscale Model

Jose Gomez-Tames* (1), Shinta Aonuma(1), Takaharu Kutsuna(1) and Akimasa Hirata(1)
(1) Department of Electrical and Mechanical Engineering, Nagoya Institute of Technology, Nagoya, Japan, 466-8555

Abstract

In brain tumor surgery, it is necessary to achieve an optimal balance between completeness of tumor resection and prevention of damage to motor function. In particular, careful planning is necessary when the tumor is in or near the motor cortex. The gold standard technique for identifying and monitoring structures of the primary motor cortex and pyramidal tract intraoperatively is direct brain stimulation (DES). Transcranial magnetic stimulation (TMS) has also been used to stimulate brain structures noninvasively in the preoperative phase. However, the exact spatial relationship between the tumor and essential motor areas needs to be determined. Thus, the stimulation mechanisms of these two techniques need to be examined and the differences between these mechanisms need to be determined. In this study, we developed a subject-specific multiscale human brain model with an embedded microscale model of neurons by using prior knowledge of the orientation of pyramidal neurons in the motor area. We confirmed the difference between the mechanisms of these two techniques by computing the electric field distribution and neuron activation in the motor area. We found TMS mapping to occur more prominently in the posterior gyral wall and DES mapping to occur more prominently in the gyral crown. The proposed approach is useful in defining activation threshold, which is useful for optimization of medical applications as well as for ensuring human safety.

1. Introduction

In brain tumor surgery, achieving an optimal balance between completeness of tumor resection and prevention of damage to motor function is necessary. The gold standard technique for intraoperative identification and monitoring of structures of the primary motor cortex and pyramidal tract is direct electrical stimulation (DES). [1]. DES stimulates the exposed brain cortex directly after craniotomy to identify the motor functions around the tumor through measurement of the motor evoked potential (MEP) or the contraction of the contralateral limb or muscle. However, DES is not useful during the planning phase and can increase operation time [2]. To overcome these problems, presurgical mapping is performed noninvasively by transcranial magnetic stimulation (TMS) [2]. TMS induces a current in the brain by means of a magnetic field generated from a coil placed and rotated in different configurations for peritumoral mapping during recording of the MEP.

The brain areas mapped by these two techniques are expected to differ to some extent owing to the following reasons. 1) The distribution of the induced electric field differs between DES and TMS (in the former technique, a radial electric field is generated from the electrode, whereas in the latter technique, the generated electric field has a strong transverse component). 2) The electric field distribution is affected by intraindividual differences introduced after craniotomy, (e.g., content of the spinal fluid, brain inflation, and removal of head tissues). 3) The activation mechanism of both techniques is different because of the difference in the directions of the induced electric field and the difference in neuron orientations (i.e., the difference in activated axons) [3]. However, this variability in mapped areas has thus far not been quantified. Moreover, activation threshold and stimulation site would be useful from the viewpoint of ensuring patient safety in accordance to the research agenda of the IEEE International Committee on Electromagnetic Safety for low-frequency electrical dosimetry. [4].

The purpose of the present study was to investigate the difference between the regions activated during DES mapping and TMS mapping. To this end, a subject-specific multiscale human head model was developed from images acquired using an MRI scanner, by means of an automatic segmentation algorithm. In this model, a micromodel of pyramidal neurons originating from the motor area was embedded based on the anatomical location of Betz cells. The computed electric field generated in the brain and its effects on neuron activation were quantified by mimicking the conditions of presurgical and intraoperative monitoring by DES and TMS.

2. Method

2.1 Anatomical Human Head Model

A model with a resolution of 0.5 mm employed in our previous study was used [5]. This model, shown in Fig. 1a, was constructed from T1- and T2-weighted MR images acquired using a 3T MRI scanner and represented in the form of a grid of cubical voxels (65.3×10^6 voxels). The model was segmented into a total of 14 tissues and body fluids (skin, fat, muscle, outer skull, inner skull, gray

matter, white matter, cerebellar gray matter, cerebellar white matter, brainstem, nuclei, ventricles, cerebrospinal fluid, and eye tissues) by using in-house software [5] equipped with the FreeSurfer brain imaging software package [6]. During DES, a craniotomy 5 cm in diameter was performed in the model to expose the hand motor area. An anodic electrode 7.5 × 7.5 mm^2 in area was placed over the hand knob, and a cathodic electrode 27.5 × 27.5 mm^2 in area was placed over the forehead. During TMS, the head model was left intact, and a figure-8 coil was oriented posterior-anterior to induce the maximum possible electric field strength in the hand knob.

2.2 Volume Conductor Model

For TMS mapping, the magnetic vector potential in each voxel of the head model was computed by FEKO, a commercial software package that is based on the method of moments (EMSS-SA, Stellenbosch, South Africa). The computed magnetic vector potential was used as input to the in-house magneto-quasi-static solver that implements the scalar potential finite difference method [7], [8] in order to calculate the electric scalar potential induced in the brain, φ, as

$$\nabla \cdot [\sigma(-\nabla\varphi - jwA_0)] = 0 \qquad (1),$$

where A_0 and σ denote the magnetic vector potential of the applied magnetic field and the tissue conductivity, respectively. The equation used to obtain the electric scalar potential generated in DES was almost identical to equation 1, the difference being that the source of the field was an electric potential that was nonzero only at the electrodes.

Equation 1 was solved iteratively by the successive-over-relaxation method and a multigrid method [7]. The electric field along the edge of the voxel was obtained by dividing the difference in the potential between the nodes of the voxel by the distance across the nodes and adding the vector potential.

The conductive properties of the tissues were modeled using the fourth-order Cole-Cole model [9] at 100 kHz. The displacement current was assumed to be negligible in comparison to the conduction current in view of the magneto-quasi-static approximation. Further, in the case of TMS, the currents induced in the human body were assumed to not perturb the external magnetic field.

2.3 Microscale model of Neurons

The effects of the extracellular electric field on nerve axons originating from the motor area are described by the following general equation [10], [11]:

$$c_m \frac{dV_{m,n}}{dt} + \sum_x g_x(V_m - V_x) - \frac{\Delta^2 V_{m,n}}{R} = \frac{\Delta^2 \varphi}{R} \qquad (2),$$

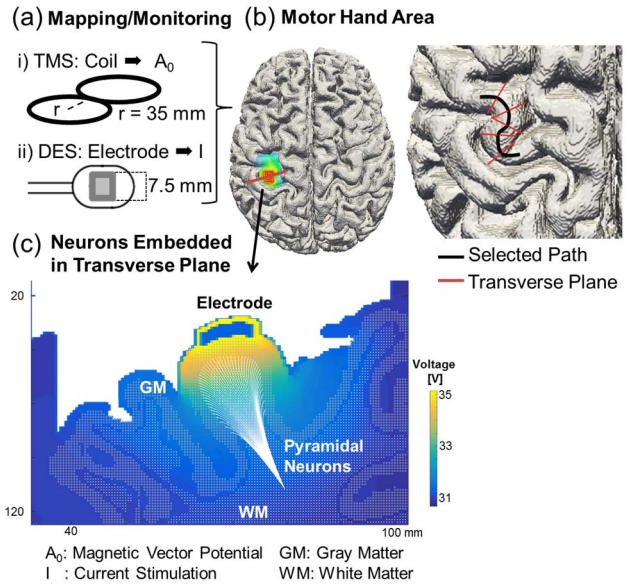

Figure 1. Multiscale model for TMS and DES. a) A realistic volume conductor model of the human head was used to study brain activation. b) Electric field targeted at the motor hand area by DES. c) Pyramidal neurons descending from the motor area were modeled using a microscale model. They were embedded in planes orthogonal to the line along the center of the gyral crown, with the bending of the axons similar to that of Betz cells.

where c_m is the membrane capacitance and $V_{m,n}$ is the membrane potential at position n along the axon. The axon of a myelinated neuron consists of internodes (segments ensheathed by myelin) and nodes of Ranvier (ionic channels) that are modeled by the conductance term g_x. At the nodes of Ranvier, the ionic membrane current depends on the dynamics of voltage-gated sodium channels and leakage channels in the nodes, which is formulated as a conductance-based voltage-gated model. In this study, the Chiu–Ritchie–Rogart–Stagg–Sweeney (CRRSS) model was considered [12]. At the myelinated internodes, the leak conductance was modeled as a passive element.

The right-hand part of equation 2 is the term $\Delta^2\varphi = \varphi(n-1) - 2\varphi(n) + \varphi(n+1)$, which describes the driving term resulting from the extracellular electrical potential. The variable R denotes the intra-axonal resistance between the centers of two adjacent compartments. The model was implemented using MATLAB 2014b to calculate the activation threshold (i.e., the lowest stimulation intensity necessary to propagate an action potential in a given neuron).

2.4 Neuron Distribution and Curvature

The curvature of the axons of pyramidal neurons that start from the motor area was considered in this study. Pyramidal neurons start from the gray matter (layers III

and IV), cross the gray–white matter interface almost perpendicularly, and descend to form the pyramidal tracts. If the pyramidal neurons start from the gyral crown, their axons will descend straight. However, if the pyramidal neurons start from the sulcal wall, their axons will bend when entering the gray matter. In our model, for a plane transverse to the motor hand area, the neurons were embedded by considering seed points located at the center of the gray matter, control points for axon bending, and end points. These three seed regions were interpolated to generate the axons of the pyramidal neurons by means of the basis-spline function of order fourth (Fig. 1c). The planes were orthogonal to a line along the center of the gyral crown (Fig. 1b). The model included 45 planes, each with 50 neuron axons 16 μm in diameter (2,250 neurons in total). Finally, the voltage distribution in the orthogonal planes was interpolated from the original volume conductor potential distribution, as shown in Fig. 1c.

3. Results

The reference position of each neuron was required for comparing their activation. This position was chosen as the intersection between the neuron axon and the gray–white matter boundary. Three-dimensional (3D) boundary lines formed according to the reference position of each axon (each line belongs to a transversal plane to the gyral crown center, as shown in Fig. 1b). The 3D boundary lines were transformed into 1D lines centered at the corresponding gyral crown. The neurons were grouped into 5 mm bins for analysis. Figure 2a shows the activation pattern during DES for stimulation thresholds that would generate an action potential in 10%, 20%, 30%, and 40% of the total neurons in the model. The neurons were activated with lower intensity when they were closer to the electrode at the precentral gyral crown. The excitation threshold increased toward deeper regions of the anterior and posterior walls. Figure 2b shows that TMS mapping was more prominent than DES mapping in the posterior gyral wall. As shown in Fig. 2c. the electric field strength distribution on the white matter surface also confirms the prominent DES mapping at the gyral crown and the prominent TMS mapping at the gyral wall.

4. Discussion

This study investigates the difference between the mapping mechanisms of TMS and DES, whose knowledge is valuable for brain tumor surgery applications. The results of DES shown in Fig. 2a can be explained by considering that the electric field is inversely proportional to the square of the distance under the assumption of a monopolar spherical electrode in an isotropic medium. In contrast, the electric field induced by TMS is transverse so activation of neurons in the posterior wall is easier (Fig. 2b). Our computational results confirm the differences between the activation mechanisms and activation areas of DES and TMS.

Quantification of the difference in activation areas for different kinds of stimulations is important, since the motor and sensory parts of the body are mapped to different brain areas. The posterior wall is related to Brodmann area 4 (motor area), whose activation can be achieved easier by aligning the handle of the figure-8 coil at approximately 45° to the parasagittal plane. The coil handle is pointed posterolaterally to induce a tissue current that flows perpendicular to the motor strip in the precentral sulcus [13]. The anterior wall is related to Brodmann area 6, which requires a different coil orientation for more optimal stimulation. Therefore, in the case of pre- and intraoperative mappings, detailed information on the activation pattern is useful for selecting optimal parameters to stimulate the region of interest. However, the representation of motor function in the brain is intermingled, which should be considered in future studies in order to investigate the significance of the activation area difference between TMS and DES.

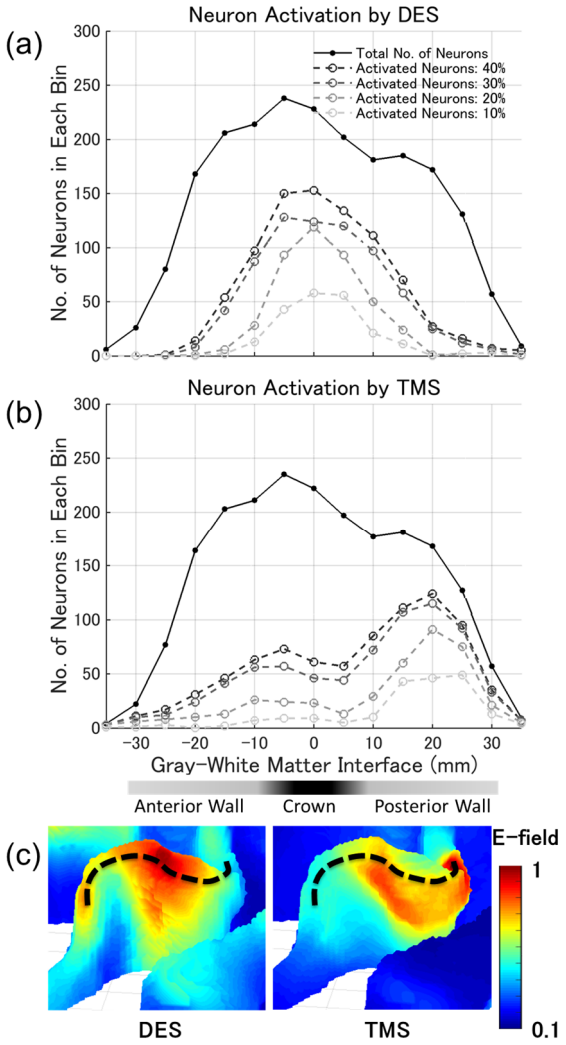

Figure 2. Activation patterns by a) DES and b) TMS, achieved by using a threshold that activates a specific percentage of the neuron population in the motor hand area. c) Normalized distribution of electric strength on

white matter surface during DES (left) and TMS (right) brain mapping. The dotted line corresponds to the selected path indicated in Fig. 1b.

In this study, on the basis of prior anatomical information, a new model was implemented that includes the bending of axons of pyramidal neurons (Fig. 1c). This model explains neuron activation by DES (a radial electric field aligned with the descending section of the axons) and that by TMS (a transverse electric field aligned with the projection of the neuron axon from gray matter and white matter). A similar approach was previously reported that was based on diffusion tensor imaging [14] for investigating the influence of TMS coil orientation. The model also confirms previous results based on the electric field strength distribution [15]. We assumed direct stimulation of the pyramidal tract axons (D-wave) for DES and TMS. During DES, D-wave occurs at the activation threshold with the patient under anesthesia, but during TMS, D-wave appears above the stimulation threshold. At the stimulation threshold, indirect trans-synaptic activation of pyramidal neurons (I1 waves) originates from gray matter and should be considered in future study [16].

5. Conclusion

Prior knowledge of the variability in brain mapping (by DES or TMS) is valuable for brain tumor surgery applications; however, this variability has not yet been determined. This study was aimed at quantifying the activation in the gyral and sulcal areas of the motor hand area during DES and TMS. To this end, a conduction model of a realistic human head that included a new microscale model of pyramidal neurons was implemented to account for the anatomical bending of these neurons, which is vital for understanding the activation mechanism of the motor area by TMS and DES. The model results confirmed that DES mapping occurs prominently in the brain cortex at the gyral crown and TMS mapping occurs prominently in that at the gyral wall.

6. Acknowledgements

This work was supported by the Ministry of Internal Affairs and Communications, Japan.

7. References

1. T. Saito, Y. Muragaki, T. Maruyama, M. Tamura, M. Nitta, and Y. Okada, “Intraoperative functional mapping and monitoring during glioma surgery.,” Neurol. Med. Chir. (Tokyo)., vol. 55, no. 1, pp. 1–13, 2015.
2. T. Picht, J. Schulz, M. Hanna, S. Schmidt, O. Suess, and P. Vajkoczy, “Assessment of the Influence of Navigated Transcranial Magnetic Stimulation on Surgical Planning for Tumors in or Near the Motor Cortex,” Neurosurgery, vol. 70, no. 5, pp. 1248–1257, May 2012.
3. L. Manola, J. Holsheimer, P. Veltink, and J. R. Buitenweg, “Anodal vs cathodal stimulation of motor cortex: A modeling study,” Clin. Neurophysiol., vol. 118, no. 2, pp. 464–474, 2007.
4. J. P. Reilly and A. Hirata, “Low-frequency electrical dosimetry: research agenda of the IEEE International Committee on Electromagnetic Safety,” Phys. Med. Biol., vol. 61, no. 12, pp. R138–R149, Jun. 2016.
5. I. Laakso, S. Tanaka, S. Koyama, V. De Santis, and A. Hirata, “Inter-subject Variability in Electric Fields of Motor Cortical tDCS,” Brain Stimul., vol. 8, no. 5, pp. 906–913, 2015.
6. A. M. Dale, B. Fischl, and M. I. Sereno, “Cortical Surface-Based Analysis,” Neuroimage, vol. 9, no. 2, pp. 179–194, Feb. 1999.
7. I. Laakso and A. Hirata, “Fast multigrid-based computation of the induced electric field for transcranial magnetic stimulation,” Phys. Med. Biol., vol. 57, no. 23, pp. 7753–7765, 2012.
8. J. Gomez-Tames, Y. Sugiyama, I. Laakso, S. Tanaka, S. Koyama, N. Sadato, and A. Hirata, “Effect of microscopic modeling of skin in electrical and thermal analysis of transcranial direct current stimulation,” Phys. Med. Biol., vol. 61, no. 24, pp. 8825–8838, Dec. 2016.
9. S. Gabriel, R. W. Lau, and C. Gabriel, “The dielectric properties of biological tissues: III. Parametric models for the dielectric spectrum of tissues,” Phys. Med. Biol., vol. 41, no. 11, pp. 2271–2293, Nov. 1996.
10. J. Gomez-Tames, J. Gonzalez, and W. Yu, “A simulation study: Effect of the inter-electrode distance, electrode size and shape in Transcutaneous Electrical Stimulation,” in Engineering in Medicine and Biology Society (EMBC), 2012, pp. 3576–3579.
11. J. Gomez-Tames, J. Gonzalez, and W. Yu, “A Simulation Study on the Dominance of the Tissues’ Conductivity in the Muscle Recruitment,” J. Med. Imaging Heal. Informatics, vol. 3, no. 1, pp. 72–78, 2013.
12. J. D. Sweeney, J. T. Mortimer, and D. Durand, “Modeling of mammalian myelinated nerve for functional neuromuscular electrostimulation,” IEEE -97th ann. conf. Eng. Med. Biol. Soc. Bost., vol. 9, pp. 1577–1578, 1987.
13. C. I. Moore, C. E. Stern, S. Corkin, B. Fischl, A. C. Gray, B. R. Rosen, and A. M. Dale, “Segregation of somatosensory activation in the human rolandic cortex using fMRI.,” J. Neurophysiol., vol. 84, no. 1, pp. 558–69, Jul. 2000.
14. A. Nummenmaa, J. A. McNab, P. Savadjiev, Y. Okada, M. S. Hämäläinen, R. Wang, L. L. Wald, A. Pascual-Leone, V. J. Wedeen, and T. Raij, “Targeting of White Matter Tracts with Transcranial Magnetic Stimulation,” Brain Stimul., vol. 7, no. 1, pp. 80–84, Jan. 2014.
15. I. Laakso, A. Hirata, and Y. Ugawa, “Effects of coil orientation on the electric field induced by TMS over the hand motor area,” Phys. Med. Biol., vol. 59, no. 1, pp. 203–218, Jan. 2014.
16. V. Di Lazzaro, A. Oliviero, P. Profice, E. Saturno, F. Pilato, A. Insola, P. Mazzone, P. Tonali, and J. C. Rothwell, “Comparison of descending volleys evoked by transcranial magnetic and electric stimulation in conscious humans.,” Electroencephalogr. Clin. Neurophysiol., vol. 109, no. 5, pp. 397–401, Oct. 1998.